Turbulence characterisation during ebbing and flooding tides in the Raz Blanchard with large eddy simulations.

Philippe Mercier, Sylvain S. Guillou, Jérôme Thiébot, and Emmanuel Poizot

Abstract—**The impact of the seabed morphology on the spatial variability of a strong tidal flow is investigated, at both flood and ebb tides, using large-eddy simulations. The simulations are performed over domains of about 0.5 km^2, with a spatial resolution of 0.34 m and using a detailed bathymetry of 1 m resolution. For both simulations, the presence of trails of reduced current velocity magnitude and high turbulence level and of trails of accelerated flow and low turbulence level is confirmed. These trails are assumed to be originated from specific seabed landforms or combinations of landforms that generate a high level of turbulence at very localised positions. The locations of the trails differ between flood and ebb tides, due to the misalignment of the flow during those two periods of the tide. On another note, the flow conditions notably differ between flood and ebb, with a large zone of low turbulence that appears during ebb tide, but not during flood tide. This is due to the difference in the upstream seabed morphology: a rough and shallow rocky plateau during flood tide and a smoother and deeper seabed during ebb tide.**

Index Terms—**Large eddy simulation, Seabed morphology, Tidal flows, Turbulence, Raz Blanchard.**

I. Introduction

KNOWLEDGE about the dynamics of extreme tidal flows increases with the growing interest for harvesting tidal power. More and more studies help increase the understanding of the hydrodynamic characteristics of the most promising sites. Initially, the focus has been put on the resource assessment and the environmental impact of turbine arrays, with analytical estimates [1], *in situ* ADCP measurements [2]–[4] and regional numerical simulations based on Reynolds Averaged Navier-Stokes models [5]–[8]. These studies confirm the huge potential of sites such as the Raz Blanchard, the Minas Passage, the Pentland Firth, or the Ramsey Sound.

On another note, many studies focus on tidal devices. They show the sensitivity of tidal turbines to turbulence, with impacts on the turbine production and wake [9]–[13] as well as an increase of the loads (and thus the fatigue) experienced by the blades [14], [15]. This sensitivity raises interest for the characterisation of ambient turbulence at tidal power sites. To investigate this issue, new ADCP configurations have emerged involving a higher number of beams (more than four beams) [16]–[18], which allows for the measurement of the full Reynolds tensors [19], [20], as well as ADV measurements [4], [21]. Also, large-eddy simulations (LES) start providing insight about the hydrodynamic characteristics of tidal and river flows [22]–[24], over large areas and with a fine spatial resolution. Such simulations are suited to a detailed assessment of the best turbine positioning. In particular, LES based on the lattice-Boltzmann method (LBM), that are less dissipative than Navier-Stokes models [25], are suited to study turbulence generation over rough seabed [26], [27].

LES are computationally expensive, which, to date, precludes investigating the whole range of tidal conditions at a given site with a fine spatial resolution. Despite this limitation, focusing on particular tidal conditions (e.g. spring tides) permits to obtain crucial information for the design and the positioning of turbines. Nevertheless, during a tide, the flow reverse and the hydrodynamic conditions can thus strongly differ during ebb and flood tides. This difference could be explained by the tidal asymmetry and/or by the asymmetric shape of the tidal channel that lead to different flow conditions depending on the orientation of the predominant current. As a consequence, studying the hydrodynamic conditions during both flood and ebb tides is crucial to have a complete view of the flow characteristics at a particular site.

Here, LES are used in the Raz Blanchard to investigate the spatial variations of the flow characteristics at both flood and ebb tides. It is noteworthy that the study zone encompasses a large and abrupt change of water depth which has a large influence of the flow. First, the area of interest is presented, as well as the numerical setup. Then, the simulated flow characteristics are presented and the impact of the seabed morphology on the turbulence is discussed.

EWTEC 2021, paper ID: 2190. This work is currently funded by the European Unit in the frame of the FCE INTERREG project TIGER.

P. Mercier is with the Laboratoire Universitaire des Sciences Appliquées de Cherbourg, Université de Caen Normandie, 60 rue Max-Pol Fouchet, 50100 Cherbourg-en-Cotentin, France (e-mail: philippe.mercier@unicaen.fr).

S. Guillou is with the Laboratoire Universitaire des Sciences Appliquées de Cherbourg, Université de Caen Normandie, 60 rue Max-Pol Fouchet, 50100 Cherbourg-en-Cotentin, France (e-mail: sylvain.guillou@unicaen.fr).

J. Thiébot is with the Laboratoire Universitaire des Sciences Appliquées de Cherbourg, Université de Caen Normandie, 60 rue Max-Pol Fouchet, 50100 Cherbourg-en-Cotentin, France (e-mail: jerome.thiebot@unicaen.fr).

E. Poizot is with the Institut National des sciences et techniques de la mer, Conservatoire National des Arts et Métiers, Boulevard de Collignon, 50110, Tourlaville, France and with the Laboratoire Universitaire des Sciences Appliquées de Cherbourg, Université de Caen Normandie, 60 rue Max-Pol Fouchet, 50100 Cherbourg-en-Cotentin, France (e-mail: emmanuel.poizot@lecnam.net)

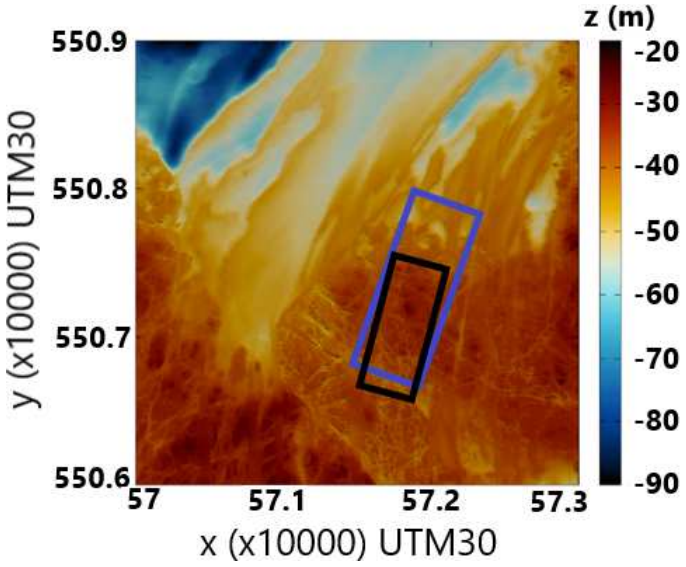

Fig. 1. Bathymetry of the investigated zone in the Raz Blanchard. The rectangles represent the simulation domains for flood (in black) and ebb (in blue).

II. Methods

A. Geomorphology and ADCP measurements

The Raz Blanchard geomorphology is diversified, with the presence of crystalline and sedimentary rocks, faults, folds, covers of blocks as well as mobile sand patches and pebble dune fields [28]. A distinction can be made between the northern part, that is deeper and smoother than the southern part. The morphology of the site is expected to impact the characteristics of the flow. In particular, we foresee that the change of depth will impact the current velocity and that the seabed roughness will influence the generation of turbulence. The maximum velocities are observed in the eastern part of the Raz Blanchard [29].

The study focuses on an area of the Raz Blanchard where two pre-commercial farms are planned to be installed (four Simec Atlantis Energy turbines by Normandie Hydroliennes and seven OceanQuest turbines by Hydroquest). The zone is situated at the frontier between the northern part of the race that is deep and composed of a smooth seabed and the southern part that is shallower and constituted of a rocky (and rough) seabed (see Figure 1), and in the eastern part of the Raz Blanchard, characterised by high velocities. ADCP measurements have been achieved in this area using two, coupled, 4-beam ADCPs [19], [20]. This configuration allows for the calculation of the full Reynolds tensor over a vertical profile, in addition to the time-mean velocity profile. The temporal evolution of the sea level over a three day period is represented in Figure 2(a). Over a full 14-days tidal cycle, the depth range varies from less than 2 m at neap tides to more than 6 m at spring tides. The maximum and minimum sea levels correspond respectively to the flood and ebb peak currents, as showed in Figure 2(b). The flow orientation is represented in Figure 2(c). It is very similar from one tidal cycle to another and roughly stable over a given flood or ebb period. This confirms the relevance of a study based on only two simulations, one for the flood and one for the ebb.

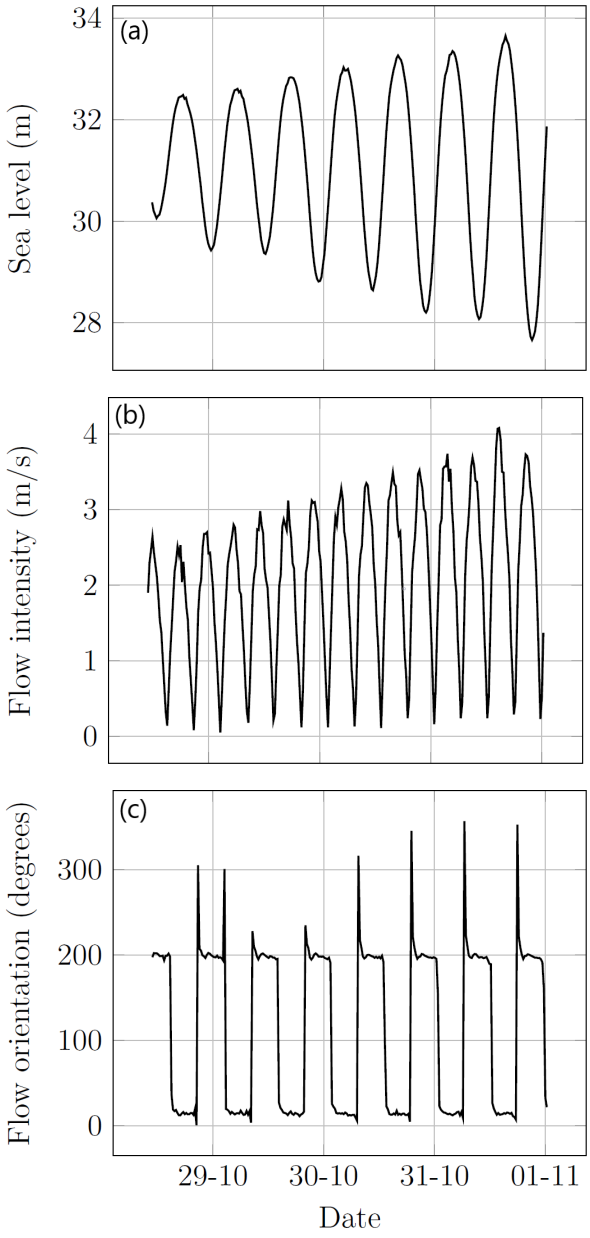

Fig. 2. Temporal evolution of (a) the sea level, (b) the flow intensity and (c) the flow orientation at the reference ADCP position.

B. LBM-LES

The LBM-LES simulations are based on the open-source C++ library Palabos [30]. The numerical parameters are similar to those retained in an earlier work [26], with a D3Q19 numerical scheme, a BGK (Bhatnagar-Gross-Krook) collision operator [31] enhanced by a regularisation procedure [32] and a static Smagorinsky model [33], [34] using a 0.14 Smagorinsky constant. The seabed is modelled with a Bouzidi no-slip condition [35]. The sea surface is considered to be flat and modelled with a free-slip condition. A Dirichlet boundary condition [36] is applied on the lateral boundaries, where the velocity is set to be constant, uniform, longitudinal and set to a magnitude of 4 m.s^{-1}. A 2 m-large sponge zone is used on

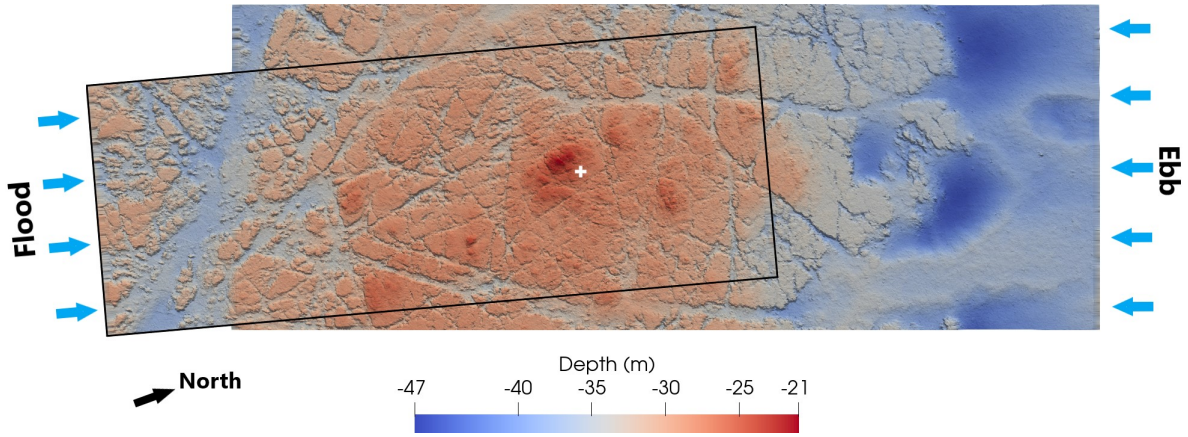

Fig. 3. Flood and ebb simulation domain. The depths are relative to the sea surface at low tide of a spring tide. The white cross indicates the position of ADCP measurements.

the lateral and top boundaries where the viscosity is artificially increased to improve the numerical stability. A previous work [27] showed that these lateral boundary conditions influence artificially the flow over a constraint distance to the boundaries (less than 40 m). A periodicity condition is applied between the outlet and the inlet. The continuity of the bathymetry is ensured by a transition zone of 20 m that connects the outlet to the inlet in a linear way. The study domain must be carefully selected for this transition. Indeed, abrupt changes of depth between the inlet and the outlet may generate artificial flow perturbations. A pressure gradient compensates the load losses. Its value is estimated from [26]. The domain is divided into two areas of different resolutions. In each area, the mesh is Cartesian. The area of finest mesh resolution (0.34 m) is situated near the seabed and the area of coarsest resolution (0.68 m) is situated near the sea surface.

C. Simulations

The simulation domain must be aligned with the predominant flow direction. This results in a 5° misalignment between flood and ebb simulation domains, as shown in Figure 3. To investigate the most energetic conditions, the reference flow conditions are spring tide peak ebb and flood conditions. The period corresponds to the maximum velocity magnitude observed during the one-month long measurement campaign (October, 6th, 2017).

1) Flood: The flood domain is 960 m long and 360 m wide, resulting in a mesh of 210 million nodes. It is characterised by a relatively homogeneous seabed morphology. The depth ranges from 47 m in a depression transverse to the domain in the upstream, to 27 m at the top of a large landform in the downstream part. Simulations on this domain has already been validated against ADCP measurements [26], [27].

2) Ebb: The simulation domain for the ebb tide notably differs from the one retained for simulating flood tide. The highest point of the bathymetry is the same landform as in the flood simulation. However, its depth is different because the flood peak happens at high tide whereas the ebb peak happens at low tide, with a 6.7 m difference in the sea level. The seabed morphology varies from a smooth and deep area (depth of 47 m) in the upstream area to a rocky and shallow area (depth of 21 m). In order to properly capture the physical phenomena occurring in both areas, the domain is extended in the longitudinal direction. Thus, the ebb simulation domain is 1240 m long and 465 m wide, resulting in a mesh of 470 million nodes. The validation of the ebb simulation against ADCP measurements is displayed in Figure 4. This figure represents a comparison of vertical profiles of longitudinal velocity and two components of the velocity variance, from ADCP measurements and from the simulation. A good agreement between the measurements and the simulation is observed, despite a slight overestimation of the flow intensity and a slight underestimation of the velocity variance in the lower part of the water column.

III. Results

The simulation results are represented in Figure 5 for the average longitudinal velocity and in Figure 6 for the variance of the longitudinal velocity. The results are given on a horizontal plane extracted 15 m under the ebb sea level. In order to visualise the results from both simulations on the same images, the results from the flood simulation are represented with iso-surfaces whereas the results from the ebb simulation are represented with iso-contours.

Regarding the average longitudinal velocity in Figure 5, it is found to be stronger in the central part of the domain, where the velocity magnitude is around 4 $m.s^{-1}$, than in the left and right extremities of the figure, where the velocity is of the order of 3 $m.s^{-1}$. This difference can be related to the variations of depth (see Figure 3), with the central part of the domain being shallower. Also, stream-oriented trails of reduced velocity magnitude and flow acceleration are observed for both simulations. They result in alternating blue and red strips that persist over the entire domain for the flood simulation. The distance between the trails ranges between 70 m and 150 m. The difference of velocity between trails of reduced speed and trails of

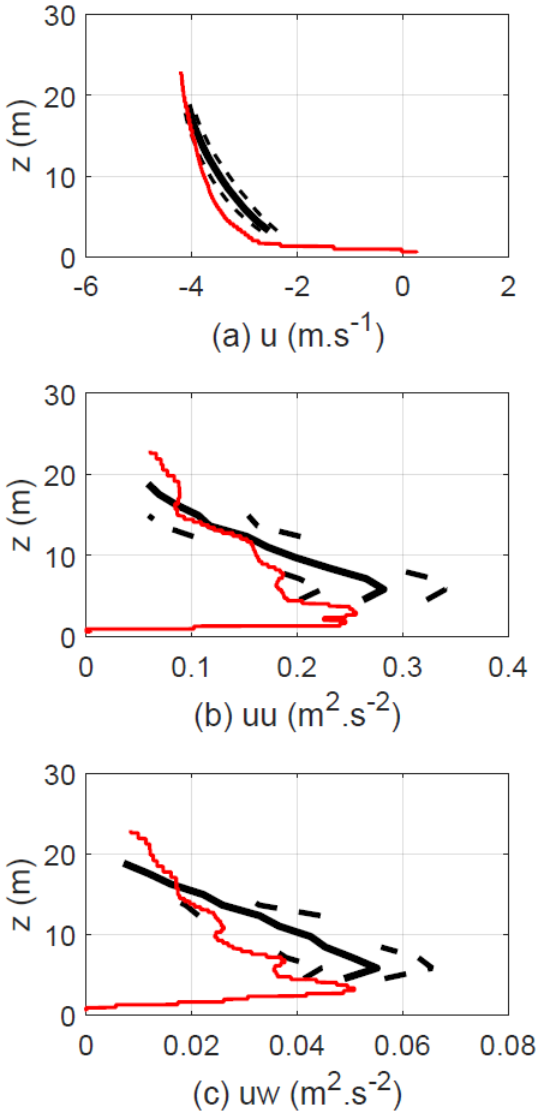

Fig. 4. Validation of the ebb simulation (—) against ADCP measurements. (—)

increased speed reaches 0.5 m.s^{-1}. Due to the misalignment between ebb and flood, the ebb trails are crossing the flood trails. Thus, under-speed zones at ebb might be over-speed zones at flood (e.g. at point A), and vice versa (e.g. at point B). At both ebb and flood tides, other zones can be characterised by an increased velocity (e.g. at point C) or by a reduced velocity (e.g. at point D). Concerning the point D, it is remarkable that the trails of under-speed passing by this point are passing just aside of the highest and largest landform of the study domain. The particular feature could thus play a role in the generation of these two under-speed trails.

Regarding the variance of the longitudinal velocity, the Figure 6 highlights trails similar to the ones observed for the longitudinal velocity. Within the trails of low turbulence, the variance of the longitudinal velocity is below 0.1 m^2.s^{-2} whereas it reaches 0.25 m^2.s^{-2} within the trails of high turbulence. It is remarkable that the high turbulence trails superimpose to the low velocity trails, and vice versa, as already observed in a previous work focusing on the flood tide [27]. Indeed, the point A in Figure 6, for example, is situated on a high turbulence trail at ebb and on a low turbulence trail at flood. It is the contrary for the point B. This observation also applies at points C and D during the flood, with a low turbulence for the point C and a high turbulence for point D. However, during ebb, the central part of the domain is characterised by a low turbulence, thus it is not possible to draw conclusions for the points C and D. This is a remarkable difference between flood, where the turbulence is globally uniform in the longitudinal direction, and ebb, where a significant drop in turbulence is observed in the central part of the domain.

IV. Discussion and conclusion

This study provides a detailed spatial mapping of the flow conditions over a large part of a tidal power site, at both flood and ebb peaks. It extends the results of previous investigations using large-eddy simulations, that focused only on one flow orientation.

The ebb simulation exhibits two zones with contrasted hydrodynamic behaviours both in terms of the velocity and the turbulence characteristics. Indeed, the upstream part of the ebb simulation domain is characterised by a deep and smooth seabed over which the flow velocity is low compared to the velocity over the shallower areas located in the southern part of the race (in the downstream part of the domain). In this zone, the current velocity magnitude is higher due to the flow constriction (shallower depth). Furthermore, the turbulence generation is higher as the seabed is very rough (mainly composed of rock outcrops). If a low flow velocity is actually observed in the deep area, the low turbulence intensity is shifted downstream and observed in the central part of the ebb simulation domain. This phenomenon can be explained by the fact that turbulence is generated near the seabed and gradually rises in the water column. Turbine developers could take advantage of this shift by installing the turbines in the area where the flow is accelerated band the turbulence is relatively low because it remains close to the seabed.

The presence of trails of reduced speed and high turbulence, and trails of over-speed and low turbulence, that has already been observed [27] is confirmed for both flood and ebb tides. Moreover, because of the 5° misalignment between flood and ebb flow orientation, the trails cross each others. Thus, some areas can be characterised by high (or low) turbulence intensity during both flood and ebb tides, whereas other areas can be characterised by a high turbulence intensity for one flow direction and by a low turbulence intensity for the other flow direction. This observation supports the importance of characterising tidal power sites for both flood and ebb, and more generally speaking, for all flow directions.

The trails of high turbulence intensity are expected to result from the wakes of specific seabed landforms. However, the identification of these landforms is not straightforward. Thus, the comparative analysis of flood and ebb simulation can help identifying the zone

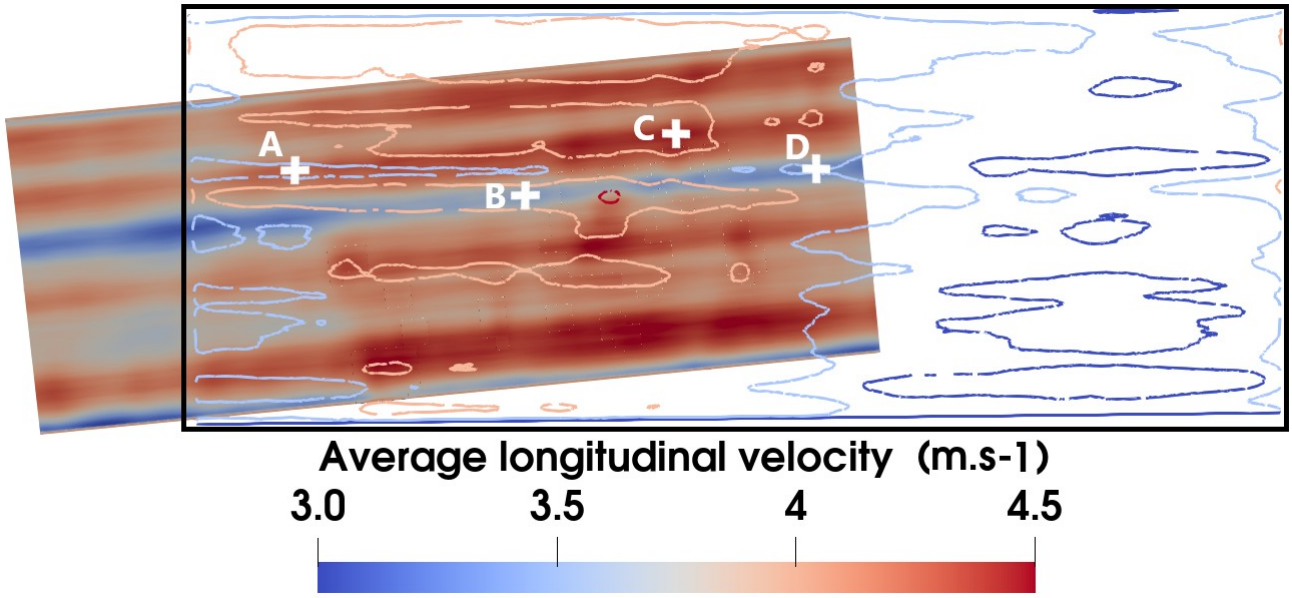

Fig. 5. Average longitudinal velocity at a 15-m depth for flood (iso-surfaces) and ebb (iso-contours).

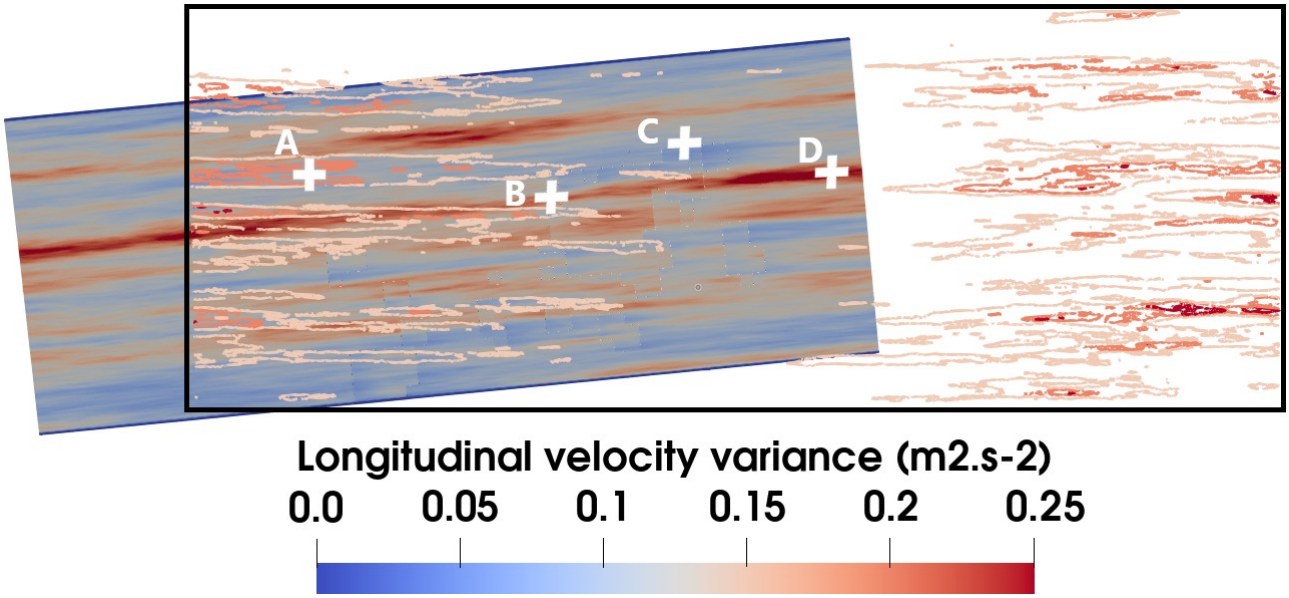

Fig. 6. Average longitudinal velocity variance at a 15-m depth for flood (iso-surfaces) and ebb (iso-contours).

of turbulence generation: it is potentially relevant to put the focus on the zones situated on high turbulence trails for both simulations.

Finally, several limitations (and potential perspectives to improve this work) are reminded:

- The seabed elevation, the flow direction and intensity are highly variable in time. Here, only two specific conditions have been investigated. Thus, it is not possible to draw firm conclusions that would apply to the whole range of tidal conditions occurring at this specific site. However, the conditions addressed here correspond to the flow peaks in flood and ebb, when the most energetic events are expected to happen.
- Because of the periodicity of the domain in the longitudinal direction, the trails of high turbulence intensity and of low velocity, that subsist over the whole length of the simulation domain, are possibly self-sustaining. Thus, the results of this study apply in a qualitative way.

ACKNOWLEDGEMENT

This work is funded by the INTERREG TIGER project. It also benefits from a French State grant managed by the National Research Agency under the Investments for the Future program bearing the reference ANR-10-IEED-0006-11. We are grateful to the CRIANN (”Centre Régional Informatique et d’Applications Numériques de Normandie”) for providing computational means, and the French navy SHOM (”Service Hydrographique et Océanographique de la Marine”) for providing access to bathymetric data (http://data.shom.fr/).

References

[1] A. Bahaj and L. Myers, "Analytical estimates of the energy yield potential from the alderney race (channel islands) using marine current energy converters," Renewable Energy, vol. 29, pp. 1931–1945, 2004. I

[2] C. Stevens, M. Smith, B. Grant, C. Stewart, and T. Divett, "Tidal energy resource complexity in a large strait: The karori rip, cook strait," Continental Shelf Research, vol. 33, pp. 100–109, 2012. [Online]. Available: https://doi.org/10.1016/j.csr.2011.11.012 I

[3] M. Togneri and I. Masters, "Micrositing variability and mean flow scaling for marine turbulence in ramsey sound," Journal of Ocean Engineering and Marine Energy, vol. 2, pp. 35–46, 2016. [Online]. Available: https://doi.org/10.1007/s40722-015-0036-0 I

[4] M. Guerra, R. Cienfuegos, J. Thomson, and L. Suarez, "Tidal energy resource characterization in Chacao Channel, Chile," International Journal of Marine Energy, vol. 20, pp. 1–16, 2017. [Online]. Available: https://doi.org/10.1016/j.ijome.2017.11.002 I

[5] R. Karsten, A. Swan, and J. Culina, "Assessment of arrays of in-stream tidal turbines in the bay of fundy," Philosophical Transactions of the Royal Society A, vol. 371, no. 20120189, 2013. [Online]. Available: http://dx.doi.org/10.1098/rsta.2012.0189 I

[6] J. Thiébot, P. Bailly du Bois, and S. Guillou, "Numerical modeling of the effect of tidal stream turbines on the hydrodynamics and the sediment transport - application to the alderney race (raz blanchard), france," Renewable Energy, vol. 75, pp. 356–365, 2015. [Online]. Available: http://dx.doi.org/10.1016/j.renene.2014.10.021 I

[7] D. S. Coles, L. S. Blunden, and A. S. Bahaj, "Assessment of the energy extraction potential at tidal sites around the channel islands," Energy, vol. 124, pp. 171–186, 2017. [Online]. Available: http://dx.doi.org/10.1016/j.energy.2017.02.023 I

[8] M. Thiébaut, A. Sentchev, and P. Bailly du Bois, "Merging velocity measurements and modeling to improve understanding of tidal stream resource in Alderney Race," Energy, vol. 178, pp. 460–470, 2019. [Online]. Available: https://doi.org/10.1016/j.energy.2019.04.171 I

[9] T. Blackmore, W. M. J. Batten, and A. S. Bahaj, "Influence of turbulence on the wake of a marine current turbine simulator," Proceedings of the Royal Society, 2014. [Online]. Available: http://dx.doi.org/10.1098/rspa.2014.0331 I

[10] M. Ahmadi, "Influence of upstream turbulence on the wake characteristics of a tidal stream turbine," Renewable Energy, vol. 132, pp. 989–997, 2019. [Online]. Available: https://doi.org/10.1016/j.renene.2018.08.055 I

[11] P. Ouro and T. Stoesser, "Impact of environmental turbulence on the performance and loadings of a tidal stream turbine," Flow, Turbulence and Combustion, 2019. [Online]. Available: https://doi.org/10.1007/s10494-018-9975-6 I

[12] M. Grondeau, S. Guillou, P. Mercier, and E. Poizot, "Wake of a ducted vertical axis tidal turbine in turbulent flows, LBM actuator-line approach," Energies, vol. 12, no. 4273, 2019. [Online]. Available: https://doi.org/10.3390/en12224273 I

[13] M. Grondeau, J.-C. Poirier, S. Guillou, Y. Méar, P. Mercier, and E. Poizot, "Modelling the wake of a tidal turbine with upstream turbulence: LBM-LES versus Navier-Stokes LES," International Marine Energy Journal, vol. 3, no. 2, 2020. [Online]. Available: https://doi.org/10.36688/imej.3.83-89 I

[14] U. Ahmed, D. Apsley, T. Stallard, and P. Stansby, "Fluctuating loads on a tidal turbine due to velocity shear and turbulence: Comparison of cfd with field data," Renewable Energy, vol. 112, pp. 235–246, 2017. [Online]. Available: http://dx.doi.org/10.1016/j.renene.2017.05.048 I

[15] B. Gaurier, P. Druault, M. Ikhennicheu, and G. Germain, "Experimental analysis of the shear flow effect on tidal turbine blade root force from three-dimensional mean flow reconstruction," Philosophical Transactions of the Royal Society A, vol. 378, no. 20200001, 2020. [Online]. Available: http://dx.doi.org/10.1098/rsta.2020.0001 I

[16] B. Vermeulen, A. Hoitink, and M. Sassi, "Coupled ADCPs can yield complete Reynolds stress tensor profiles in geophysical surface flows," Geophysical Research Letters, vol. 38, no. L06406, 2011. [Online]. Available: https://doi.org/10.1029/2011GL046684 I

[17] M. Togneri, D. Jones, S. Neill, M. Lewis, S. Ward, M. Piano, and I. Masters, "Comparison of 4- and 5-beam acoustic doppler current profiler configurations for measurement of turbulent kinetic energy," Energy Procedia, vol. 125, pp. 260–267, 2017. [Online]. Available: https://doi.org/10.1016/j.egypro.2017.08.170 I

[18] E. Droniou, M. Folley, Y. Perignon, and C. Boake, "Advanced measurement and analysis of waves and turbulence using 5-, 7- or 8-beam ADCPs," in Proceedings of the 13th European Wave and Tidal Energy Conference 1-6 Sept 2019, Naples, Italy, 2019. I

[19] M. Thiébaut, J.-F. Filipot, C. Maisondieu, G. Damblas, A. Pieterse, R. Duarte, E. Droniou, N. Chaplain, and S. Guillou, "Assessing the turbulent kinetic energy budget in an energetic tidal flow from coupled ADCPs measurements," Philosophical Transactions of the Royal Society A, 2020. [Online]. Available: https://doi.org/10.1098/rsta.2019.0496 I, II-A

[20] M. Thiébaut, J.-F. Filipot, C. Maisondieu, G. Damblans, C. Jochum, L. Kilcher, and S. Guillou, "Characterization of the vertical evolution of the three-dimensional turbulence for fatigue design of tidal turbines," Philosophical Transactions of the Royal Society A, vol. 378, no. 20190495, 2020. [Online]. Available: http://dx.doi.org/10.1098/rsta.2019.0495 I, II-A

[21] J. Thomson, B. Polagye, V. Durgesh, and M. Richmond, "Measurements of turbulence at two tidal energy sites in puget sound, wa," IEEE Journal of oceanic engineering, vol. 37, no. 3, 2012. [Online]. Available: https://doi.org/10.1109/JOE.2012.2191656 I

[22] E. Zangiabadi, M. Edmunds, I. Fairley, M. Togneri, A. Williams, I. Masters, and N. Croft, "Computational fluid dynamics and visualisation of coastal flows in tidal channels supporting ocean energy development," Energies, vol. 8, pp. 5997–6012, 2015. [Online]. Available: https://doi.org/doi:10.3390/en8065997 I

[23] T. Le, A. Khosronejad, F. Sotiropoulos, N. Bartelt, S. Woldeamlak, and P. Dewall, "Large-eddy simulation of the Mississippi River under base-flow condition: hydrodynamics of a natural diffluence-confluence region," Journal of Hydraulic Research, 2018. [Online]. Available: https://doi.org/10.1080/00221686.2018.1534282 I

[24] A. Bourgoin, S. Guillou, J. Thiébot, and R. Ata, "Turbulence characterization at a tidal energy site using large-eddy simulations: case of the Alderney Race," Philosophical Transactions of the Royal Society A, vol. 378, no. 20190499, 2020. [Online]. Available: https://doi.org/10.1098/rsta.2019.0499 I

[25] S. Marié, D. Ricot, and P. Sagaut, "Comparison between lattice boltzmann method and navier-stokes high order schemes for computational aeroacousitcs," Journal of Computational Physics, vol. 228, pp. 1056–1070, 2009. [Online]. Available: https://doi.org/10.1016/j.jcp.2008.10.021 I

[26] P. Mercier, M. Grondeau, S. Guillou, J. Thiébot, and E. Poizot, "Numerical study of the turbulent eddies generated by the seabed roughness. Case study at a tidal power site," Applied Ocean Research, vol. 97, no. 102082, 2020. [Online]. Available: https://doi.org/10.1016/j.apor.2020.102082 I, II-B, II-B, II-C1

[27] P. Mercier and S. Guillou, "The impact of the seabed morphology on turbulence generation in a strong tidal stream," Physics of Fluids, vol. 33, no. 055125, 2021. [Online]. Available: https://doi.org/10.1063/5.0047791 I, II-B, II-C1, III, IV

[28] L. Furgerot, Y. Poprawski, M. Violet, E. Poizot, P. Bailly du Bois, M. Morillon, and Y. Méar, "High-resolution bathymetry of the alderney race and its geological and sedimentological description (raz blanchard, northwest france)," Journal of Maps, vol. 15, pp. 708–718, 2019. [Online]. Available: https://doi.org/10.1080/17445647.2019.1657510 II-A

[29] P. Bailly du Bois, F. Dumas, M. Morillon, L. Furgerot, C. Voiseux, E. Poizot, Y. Méar, and A.-C. Bennis, "The alderney race: general hydrodynamic and particular features," Philosophical Transactions of the Royal Society A, vol. 378, no. 20190492, 2020. [Online]. Available: http://dx.doi.org/10.1098/rsta.2019.0492 II-A

[30] J. Latt, O. Malaspinas, D. Kontaxakis, A. Parmigiani, D. Lagrava, F. Brogi, M. B. Belgacem, Y. Thorimbert, S. Leclaire, S. Li, F. Marson, J. Lemus, C. Kotsalos, R. Conradin, C. Coreixas, R. Petkantchin, F. Raynaud, J. Beny, and B. Chopard, "Palabos: Parallel lattice boltzmann solver," Computers Mathematics with Applications, 2020. II-B

[31] P. Bhatnagar, E. Gross, and M. Krook, "A model for collision processes in gases," Physical Review, vol. 94, no. 3, 1954. [Online]. Available: http://dx.doi.org/10.1103/PhysRev.94.511 II-B

[32] J. Latt and B. Chopard, "Lattice Boltzmann method with regularized pre-collision distribution functions," Mathematics and Computers in Simulation, vol. 72, pp. 165–168, 2006. [Online]. Available: https://doi.org/10.1016/j.matcom.2006.05.017 II-B

[33] J. Smagorinsky, "General circulation experiments with the primitive equations," Monthly Weather Review, vol. 91, no. 3,

pp. 99–164, 1963. [Online]. Available: https://doi.org/10.1175/1520-0493(1963)091⟨0099:GCEWTP⟩2.3.CO;2 II-B

[34] J. Eggels and J. Somers, "Numerical simulation of free convective flow using the lattice-Boltzmann scheme," International Journal of Heat and Fluid Flow, vol. 16, no. 5, 1995. [Online]. Available: https://doi.org/10.1016/0142-727X(95)00052-R II-B

[35] M. Bouzidi, M. Firdaouss, and P. Lallemand, "Momentum transfer of a Boltzmann-lattice fluid with boundaries," Physics of Fluids, vol. 13, no. 3452, 2001. [Online]. Available: https://doi.org/10.1063/1.1399290 II-B

[36] Q. Zou and X. He, "On pressure and velocity boundary conditions for the lattice boltzmann bgk model," Physics of Fluids, 1997. II-B